SYSTEMS SCIENCE & CONTROL ENGINEERING: AN OPEN ACCESS JOURNAL
2024, VOL. 12, NO. 1, 2343303
https://doi.org/10.1080/21642583.2024.2343303

Indirect tuning of a complementary orientation filter using velocity data and a genetic algorithm

Dariusz Maton[a], John T. Economou[a], David Galvão Wall[a], Irfan Khan[a], Robert Cooper[a], David Ward[b] and Simon Trythall[b]

[a]Centre for Defence Engineering, Cranfield University, Defence Academy of the United Kingdom, Shrivenham, UK; [b]BAE Systems, Rochester, UK

ABSTRACT

In this paper, the accuracy of inertial sensor orientation relative to the level frame is improved through optimal tuning of a complementary filter by a genetic algorithm. While constant filter gains have been used elsewhere, these may introduce errors under dynamic motions when gyroscopes should be trusted more than accelerometers. Optimal gains are prescribed by a Mamdani fuzzy rule base whose membership functions are found using a genetic algorithm and experimental data. Furthermore, model fitness is not based directly on orientation but the error between estimated and ground truth velocities. This paper has three interrelated novel elements. The main novelty is the indirect tuning method, which is simple, low-cost and requires a single camera and inertial sensor. The method is shown to increase tracking accuracy compared with popular baseline filters. Secondary novel elements are the bespoke genetic algorithm and the time agnostic velocity error metric. The contributions from this work can help improve the localization accuracy of assets and human personnel. This research has a direct impact in command and control by improving situational awareness and the ability to direct assets to safe locations using safer routes. This results in increasing safety in applications such as firefighting and battlespace.

ARTICLE HISTORY
Received 18 December 2023
Accepted 9 April 2024

KEYWORDS
Inertial measurement unit; orientation filter; dead reckoning; gain optimization; complementary filter

1. Introduction

The ability to track the position of humans and vehicles under global navigation satellite system (GNSS) denial is in high demand. By 2050 for instance, it is estimated that almost 70% of the world's population will live in urban areas where multipath and signal attenuation can distort or null range measurements crucial for localization (Ritchie & Roser, 2018). A lack of accurate localization and position tracking of emergency responders can be particularly serious and, in some cases, have fatal consequences (Fire Brigades Union, 2007; Vatter, 2022). Furthermore, the vulnerability of GNSS to spoofing and jamming presents problems in the use of uninhabited aerial systems (UASs) for maritime patrol and critical infrastructure inspection (Lee et al., 2016).

While other positioning technologies exist such as those based on ultrawideband (UWB), wireless fidelity, radio frequency tags and photodiodes, they all rely on the pre-deployment of certain components into the environment beforehand. Although visual odometry (VO) systems track natural features, these are not always visible in the camera frame such as when operating in poorly lit and harsh environments (Cai et al., 2020; Wong et al., 2018; Zhang et al., 2022).

In contrast, inertial sensors are autonomous sensors which do not require any supporting infrastructure for their operation (Noureldin et al., 2013). These typically include accelerometers and gyroscopes, measuring the specific force and angular velocity of the sensor body frame, b, relative to the inertial reference frame, i, denoted $\mathbf{f}_{ib}^{b} \in \mathbb{R}^3$ and $\boldsymbol{\omega}_{ib}^{b} \in \mathbb{R}^3$, respectively. Low-cost inertial measurement units (IMUs) usually contain triads of mutually orthogonal accelerometers and gyroscopes. Unlike GNSS however, position cannot be estimated in an absolute sense but relative to a known initial position by a process of dead reckoning such as strapdown inertial navigation.

1.1. Strapdown inertial navigation

In strapdown inertial navigation, gravity-compensated acceleration expressed in the navigation frame, $\mathbf{a}_{nb}^{n} \in \mathbb{R}^3$, is double integrated with respect to known initial conditions. The navigation frame, n, is the reference frame

CONTACT Dariusz Maton d.maton@cranfield.ac.uk

pointing east, north, up. Under the assumptions of local geographic navigation and assuming initial conditions are known, position in the navigation frame, $\mathbf{x}^n_{nb} \in \mathbb{R}^3$, can be estimated by

$$\mathbf{x}^n_{nb} = \iint_{t_0}^{t} \mathbf{a}^n_{nb} \mathrm{d}t\mathrm{d}t = \iint_{t_0}^{t} (\mathbf{R}^n_b \mathbf{f}^b_{nb} + \mathbf{g}_n) \mathrm{d}t\mathrm{d}t. \quad (1)$$

In (1), $\mathbf{R}^n_b \in G$ is the rotation matrix giving the orientation of the sensor body frame relative to the navigation frame and $G = SO(3)$ is the three-dimensional Lie group. $\mathbf{f}^b_{nb} \in \mathbb{R}^3$ is a vector of accelerometer measurements (assuming the navigation frame is inertial), $\mathbf{g}_n \in \mathbb{R}^3$ is the gravity vector in the navigation frame and $t \in \mathbb{R}^+$ is time.

This method benefits from being grounded in the laws of motion and thus generalizes to all types of motion. Applying strapdown inertial navigation to low-cost sensors, however, results in a positional error that grows proportionally with t^3 due to their poor noise characteristics, bias and scale factor stabilities. In contrast, the method works well for navigation and strategic grade sensors although these are orders of magnitude more expensive (El-Sheimy & Youssef, 2020).

1.2. The importance of orientation

From (1), the implicit reliance on $\mathbf{R}^n_b$ for the accuracy of $\mathbf{x}^n_{nb}$ is shown. While there are many systematic errors affecting $\mathbf{R}^n_b$ such as inertial sensor calibration (bias and scale factor) errors and their variation with temperature (Gang-Qiang et al., 2023), the sub-optimal tuning of the orientation filter can also lead to errors. Many filters exist in literature including those based on Kalman Filtering (KF) (Barrau & Bonnabel, 2017; Bonnabel, 2007), complementary filtering (Mahony et al., 2005, 2008) and optimization (Madgwick et al., 2011; Tian et al., 2013). Here, a version of the complementary filter is used as it has been shown to be approximately five times less computationally expensive than Kalman-based methods (Michel et al., 2017). KFs, particularly the extended form (EKF), can also diverge when the linearization assumption is invalid (Skoglund et al., 2015).

In 2018, Ludwig demonstrated optimal tuning of a complementary filter using a genetic algorithm (GA). The same year, Ludwig and Jiménez (2018) used particle swarm optimization (PSO) for the same problem. However, both assumed that the optimal gain was constant and not adaptive to varying dynamics. In 2017, Poddar et al. used PSO to find adaptive optimal gains of a complementary filter however the adaptive mechanism used thresholding to switch between pre-defined gain values rather than a continuous function. The gains prescribed were therefore not necessarily optimal over the entirety of the input domain. Earlier in 2012, Shen et al. proposed an optimization method of tuning the fuzzy system regulating the gain of a complementary filter, but tuning was based on accurate knowledge of the true orientations from a more expensive tactical grade sensor. In contrast, the work presented in this paper demonstrates the ability of tuning indirectly, that is without knowledge of the true sensor orientations, using a low-cost IMU. This distinguishes it from the work of Kottath et al. published in 2017. The method is beneficial in a contested environment where windows of GNSS are available. By tuning the orientation filter, the method allows for longer inertial position tracking without GNSS updates.

The main contribution of this paper is:

(1) The prescription of optimal gains to the complementary filter by a Mamdani fuzzy inference system (FIS), whose membership functions (MF) are found by indirect optimization, that is, without explicit knowledge of the true sensor orientation.

Through this, two further contributions arising are:

(2) The design of a bespoke GA for finding the optimal rule base parameters which is shown to be faster than existing GAs for the task.

(3) Introduction of the weighted relative velocity error (WRVE), which improves on the mean square velocity error (MSVE) being a time-agnostic error metric that also accounts for the rate of turn and vibration in its evaluation.

The remainder of the paper is structured as follows. Section 2.1 introduces the complementary filter followed by its novel tuning using a GA-designed fuzzy rule base in Section 2.2. Section 2.3 introduces the novel WRVE metric and Section 2.4, the acquisition of simulation and experimental data. The results in Section 3 show the error reduction in velocity and position estimates thanks to optimization. The performance of the method subject to disturbances in explored as well as the effect of using a higher quality sensor. A discussion of the results is presented followed by a conclusion in Sections 4 and 5, respectively.

2. Method

2.1. Complementary orientation filter

Complementary orientation filters are nonlinear obser vers that estimate the orientation of the sensor body frame relative to the local level frame (Nazarahari & Rouhani, 2021). As model-free filters, they do not require

a complex mathematical model making them widely applicable and computationally tractable (El-Kebir & Ornik, 2020). The complementary filter operating principle involves high and low pass filtering the gyroscope and accelerometer measurements respectively to obtain more accurate estimates.

While other sensors such as magnetometers can be used for the observation of geomagnetic north (Renaudin et al., 2012), due to interference from hard and soft iron biases in indoor environments, the filter used in this work was limited to gyro and accelerometer measurements. Thus, while previously measurements were relative to the navigation frame, the equations below refer to the locally level frame, *l*, as north was not observable but defined by the gyroscopes at initialization. For compactness and computational efficiency, quaternion parametrization was used.

The complementary filter tuned in this work resembled the passive filter described by Mahony et al. (2008). The initialized or previous orientation estimate, expressed as a unit norm quaternion, $\hat{\mathbf{q}}_b^l$, evolved with the gyroscope measurements according to:

$$\dot{\mathbf{q}}_b^l = 1/2\hat{\mathbf{q}}_b^l \otimes \begin{bmatrix} 0 \\ \boldsymbol{\omega}_{lb}^b \end{bmatrix} \tag{2}$$

where $\hat{\mathbf{q}}_b^l \in \mathbb{H}$ and $\otimes$ is the quaternion product. This was discretized according to the Euler-Rodrigues formula:

$$\mathbf{q}_{b_{k+1}}^l = \hat{\mathbf{q}}_{b_k}^l \otimes \begin{bmatrix} \cos||\Delta t/2\boldsymbol{\omega}_{lb_{k+1}}^b||_2 \\ \hat{\boldsymbol{\omega}}_{lb_{k+1}}^b \sin||\Delta t/2\boldsymbol{\omega}_{lb_{k+1}}^b||_2 \end{bmatrix} \tag{3}$$

where $||||_2$ is the Euclidean norm and $k \in \mathbb{N}$ are the epochs. Owing to the limited sensitivity of low-cost MEMS IMUs, the assumptions $\boldsymbol{\omega}_{ib}^b \simeq \boldsymbol{\omega}_{lb}^b$ and $\mathbf{f}_{ib}^b \simeq \mathbf{f}_{lb}^b$ were made. That is, the locally level frame was assumed to be inertial.

While (2) evolved orientation with the gyro measurements, the attitude (pitch and roll) update from the accelerometers to correct for drift needed to be included. Mahony et al. proposed the addition of a scaled error term, $k_p\boldsymbol{\varepsilon}_k$, to the gyroscope measurements and the same approach was used here:

$$\boldsymbol{\omega}_{\text{corr}} = \boldsymbol{\omega}_{lb_{k+1}}^b + k_p\boldsymbol{\varepsilon} \tag{4}$$

where $\boldsymbol{\omega}_{\text{corr}} \in \mathbb{R}^3$ are the corrected angular velocities, $k_p \in \mathbb{R}^+$ is the proportional angular error gain and $\boldsymbol{\varepsilon} \in \mathbb{R}^3$ is the angular velocity error vector. Based on the complementary filter described by Madgwick et al. (2020), $\boldsymbol{\varepsilon}$ was calculated by the cross product between the true gravity vector in the sensor body frame, $\mathbf{f}_{lb}^b$ measured by the accelerometers, and its predicted projection in the body frame based on the current orientation estimate, $\hat{\mathbf{q}}_{b_k}^l$:

$$\boldsymbol{\varepsilon} = \mathbf{f}_{lb}^b \times \left(\hat{\mathbf{q}}_{b_k}^l \otimes \begin{bmatrix} 0 \\ 0 \\ 1 \end{bmatrix} \otimes \hat{\mathbf{q}}_{b_k}^{l*} \right) \tag{5}$$

In (5), $*$ is the quaternion conjugate and $\times$ the vector cross product. The cross product gave a vector orthogonal to those on the right-hand side of (5). $\boldsymbol{\varepsilon}$ was thus an approximation of the tangent space of S^3 at the subgroup's identity. Figure 1 shows a diagram of the complementary filter.

The error term, $\boldsymbol{\varepsilon}$, was not necessarily accurate, however:

(1) The accelerometers giving $\mathbf{f}_{lb}^b$ required accurate calibration to ensure they represented the true gravity vector in the sensor body frame. While static calibration methods may have given bias and scale factor parameters, changes in sensor temperature would have invalidated these.
(2) Since the accelerometers measured the vector sum of all proper accelerations relative to the inertial frame, $\mathbf{f}_{lb}^b$ was polluted with additional accelerations when in motion which were not representative of attitude. Hence, although constant k_p was proposed by Madgwick et al. (2020), accurate orientation estimation required the gain to be tuned.

This work addresses the latter of these while the former is left as a topic of future work. The following constitutes the novel contribution to the field.

2.2. Tuning using the GA

The tuning of the proportional filter gain, k_p, was encoded in a single input single output (SISO) Mamdani fuzzy rule base (type 1). A type 1 model was chosen as it produced a simpler and more interpretable model which is better suited in engineering applications (Martínez-Soto et al., 2015).

The input for the classifier was the L2 norm of the angular velocity measurements from the gyros, $||\boldsymbol{\omega}_{lb}^b||_2$, $||\boldsymbol{\omega}||$ hereon. This choice of input feature was justified as gyro measurements have been reported better indicators of motion than accelerometer measurements (Yun et al., 2007). The single output was the proportional gain, k_p.

While the fuzzy rule base could have been designed manually, it was difficult to guarantee optimal tuning as the number of MFs, their shapes and positions over the input-output domains offered an exponential number of combinations. By assuming a rule base with four Gaussian MFs encoding input-output relations for still, low, high

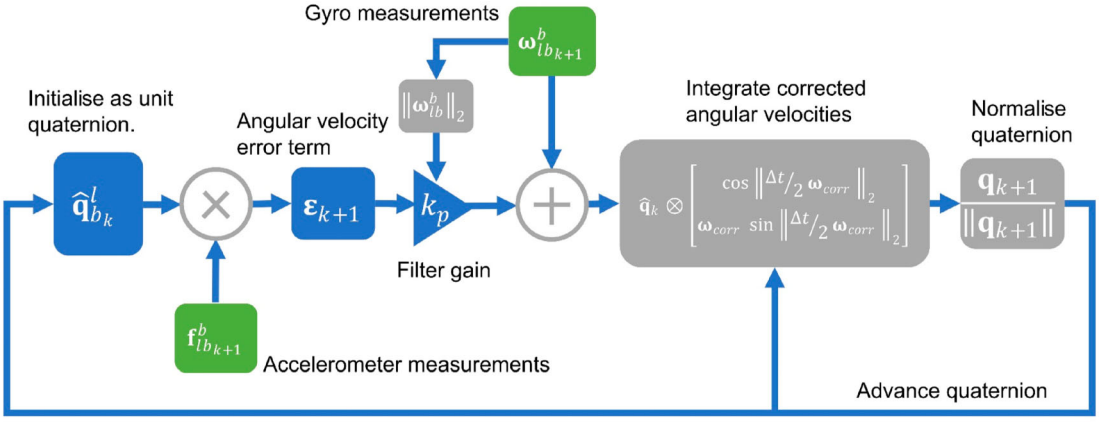

Figure 1. Complementary filter diagram.

and very high motion, the parameter set for tuning k_p was defined as:

$$\begin{aligned}\boldsymbol{\theta} = \{&\sigma_{||\boldsymbol{\omega}||_{\text{still}}}, \sigma_{||\boldsymbol{\omega}||_{\text{low}}}, \sigma_{||\boldsymbol{\omega}||_{\text{high}}}, \sigma_{||\boldsymbol{\omega}||_{v.\text{high}}},\\ &\sigma_{k_{p,v.\text{low}}}, \sigma_{k_{p,\text{low}}}, \sigma_{k_{p,\text{high}}}, \sigma_{k_{p,v.\text{high}}}, \ldots\\ &\mu_{||\boldsymbol{\omega}||_{\text{still}}}, \mu_{||\boldsymbol{\omega}||_{\text{low}}}, \mu_{||\boldsymbol{\omega}||_{\text{high}}}, \mu_{||\boldsymbol{\omega}||_{v.\text{high}}},\\ &\mu_{k_{p,v.\text{low}}}, \mu_{k_{p,\text{low}}}, \mu_{k_{p,\text{high}}}, \mu_{k_{p,v.\text{high}}}\}\end{aligned} \tag{6}$$

where $\sigma \in \mathbb{R}^+$ denotes standard deviation of the Gaussian MF and $\mu \in \mathbb{R}$, its mean. Certain assumptions were applied to the parameter search, such as intuitively fixing $\mu_{||\boldsymbol{\omega}||_{\text{still}}}$ at 0 rads^{-1}. The input and output domains were also bounded between [0, 4.36] rads^{-1} and [0, 0.1] respectively. While the upper bound of the latter was arbitrary, the former was defined by the maximum gyro output rate set on the low-cost MPU-6050 IMU to 250°s^{-1} (4.36 rads^{-1}).

Though a grid search could be used for optimizing the rule base, such enumerative methods are computationally expensive with the number of iterations scaling according to $O(n^m)$ for $n \in \mathbb{N}$ values for each of the $m \in \mathbb{N}$ parameters. A GA was therefore used as its implicit parallelism offered a more efficient search method. Although computationally cheaper calculus methods exist, for a solution surface with many local minima, the minimum returned may not be the global minimum (Goodfellow et al., 2016). For the 16-dimensional problem in this work, a solution surface with many local minima was assumed.

Table 1 compares the bespoke GA performance with two other implementations, MATLAB and SpeedyGA (Keki Burjorjee, 2010; MATLAB, 2024). The online, ε_{on} and offline, ε_{off} errors were based on metrics defined in De Jong (1975).

The bespoke GA was found to compute generations, $\bar{T}_{av}$, faster than the MATLAB and SpeedyGA implementations though with slightly higher online error. Code for the bespoke GA can be found in the data availability statement.

Table 1. Performance comparison for three GAs.

GA	ε_{on} (ms^{-1})	ε_{off} (ms^{-1})	$\bar{T}_{\text{av}}$ (s)
Bespoke	0.68	0.56	7.60
MATLAB	0.64	0.56	8.10
SpeedyGA	0.64	0.56	8.50

To determine the fitness of a generation, the true orientation of the body frame relative to the locally level frame was not used. Instead, a function calculated the MSVE between estimated, $\mathbf{v}^l_{lb,IMU}$ and ground truth, $\mathbf{v}^l_{lb,true}$ in the locally level frame as shown in (7) and (8).

$$\text{MSVE} = 1/n \sum_{i=1}^{n} (\mathbf{v}^l_{lb,\text{ true}} - \mathbf{v}^l_{lb,\text{IMU}})^2 \tag{7}$$

$$\mathbf{v}^l_{lb,\text{IMU}} = \int_{t_0}^{t} \left(\hat{\mathbf{q}}^l_{b_k} \otimes \begin{bmatrix} 0 \\ \mathbf{f}^b_{lb} \end{bmatrix} \otimes \hat{\mathbf{q}}^{l\,*}_{b_k} \right) + \mathbf{g}_l dt \tag{8}$$

where $\hat{\mathbf{q}}^l_{b_k}$ is the output from the orientation filter and hence, affected by the tuning of the parameters (chromosomes) in (6) by the GA. The relation between the chromosomes of the genome and fitness was thus indirect but offered a simple, low-cost method of obtaining experimental ground truth data.

Owing to velocity errors induced due to integral drift, a zero-velocity update (ZUPT) routine was used to retroactively correct integrated velocities over motion periods (Wahlstrom & Skog, 2021). The function that implemented this can be found in the data availability statement (Figure 2).

2.3. Weighted relative velocity error (WRVE) metric

While the MSVE can be used to evaluate the accuracy of velocity estimation, it had several shortcomings when

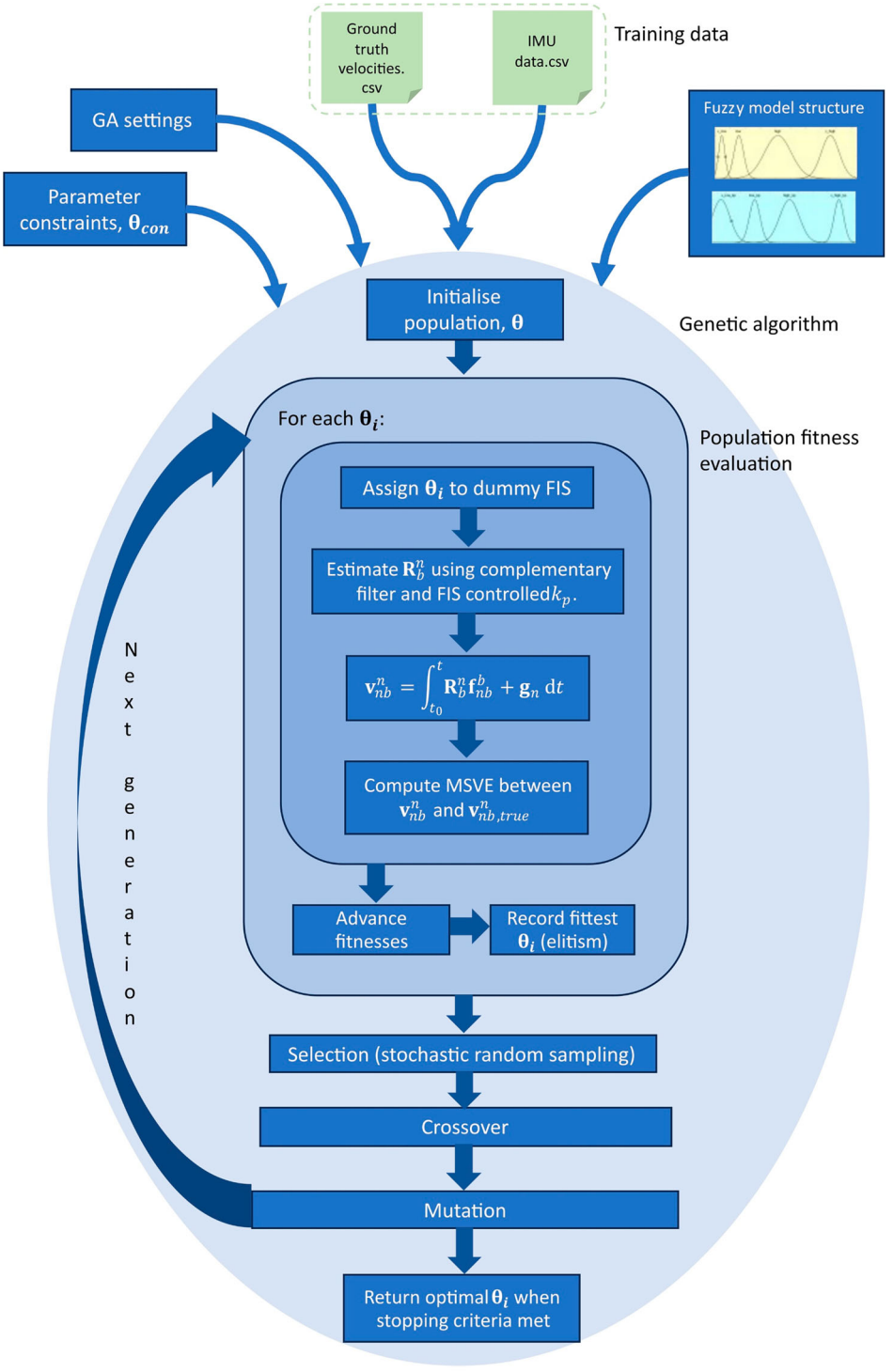

Figure 2. Overview of k_p tuning process using FIS, complementary filter and GA.

applied to the inertial tracking problem. It did not consider rate of turn and vibrations which low-cost inertial sensors are known to be sensitive to and had a temporal dependency which penalized rotational errors that occurred earlier in a sequence compared to those occurring later (Groves, 2015). These were addressed by the WRVE introduced here.

Time agnosticism of the WRVE was achieved by computing the velocity error, $\boldsymbol{\varepsilon}_v \in \mathbb{R}$, over a series of windows, $\delta \in \mathbb{Z}^+$, whose lengths varied from one up to the entire sequence length. This was like the relative pose error outlined by Zhang and Scaramuzza (2018) whereby for a given $\delta_i \subseteq \delta$, the estimated trajectory segment was first aligned to the ground truth. The relative velocity error

(RVE) was thus defined as the mean of the root mean square velocity errors for each δ_i.

The WRVE was made by weighting the RVE with a velocity error vector, $\mathbf{k}_{\text{tot}} \in \mathbb{R}^+$, as shown in (9), which was calculated as the sum of the rate of turn and vibration error terms $\mathbf{k}_{\text{turn}} \in \mathbb{R}^+$ and $k_{\text{vib}} \in \mathbb{R}^+$ shown in (10):

$$\boldsymbol{\varepsilon}_v = \mathbf{k}_{\text{tot}}(\mathbf{v}_{\text{true}} - \mathbf{v}_{\text{est}}) \tag{9}$$

$$\mathbf{k}_{\text{tot}} = \mathbf{k}_{\text{turn}} + k_{\text{vib}} \tag{10}$$

where $\mathbf{k}_{\text{turn}}$ is a vector of length equal to δ_i calculated as the natural exponent of the normalized angular velocity as shown in (11):

$$\mathbf{k}_{\text{turn}} = e^{c_{\text{turn}}||\hat{\omega}||} \tag{11}$$

Higher turn rates thus exponentially increased k_{turn}. The constant $c_{\text{turn}} \in \mathbb{R}$ was set to one but is user tunable and can be made negative to make the metric more forgiving of velocity errors at higher turn rates.

k_{vib} was determined from the fast Fourier transform of normalized angular velocities over the given trajectory segment δ_i. $\bar{V} \in \mathbb{R}^+$, termed the vibrational content over the segment, was defined as the mean of the product of the single-sided power spectrum and the frequency domain up to the Nyquist limit. This was scaled by the user-defined constant $c_{\text{vib}} \in \mathbb{R}$ as shown in (12). A value of 10 for c_{vib} was used in this work.

$$k_{\text{vib}} = c_{\text{vib}}\bar{V} \tag{12}$$

$\bar{V}$ thus increased k_{vib} for signal powers closer to the Nyquist limit, and therefore penalized trajectory errors occurring at higher frequencies in the sequence. The metric was designed in this way as inputs at frequencies above the Nyquist limit get aliased down to lower frequencies and propagate as errors in the dead reckoning process.

Although the focus of the results is on the WRVE values, MSVE values are also given for comparison with results in the literature.

2.4. Acquisition of simulated and experimental data

The tuning method required the capture of synchronized IMU sensor data and ground truth velocity for an object moving in the locally-level frame.

First, synthetic IMU and velocity data were used to test the method before using experimental data. These were generated in MATLAB and, to accurately model low-cost IMU characteristics, the data sheet of the lost-cost MPU-6050 IMU was consulted. Furthermore, to best capture their noise errors, an Allan variance analysis was performed on three MPU-6050 IMUs. The mean of the bias instability, noise density and rate random walk parameters are shown in Table 2.

Simulated trajectories were generated using MATLAB's waypoint trajectory generator. To replicate the experimental data, these were confined to motions in the *x*-*y* plane and sampled at 100 Hz. Six simulation trajectories were generated: square, straight, left turn, right turn, s-shape and zigzag as shown in Figure 3(a)–(f).

The simulation trajectories had different scales, some with gentle turns such as (c) and (d) while others exhibited sharper turns like (a), (e) and (f). This was to demonstrate the efficacy of the proposed method over a variety of turn rates and the benefits of the WRVE metric.

To observe the effects of vibration on trajectories, disturbances were added to the simulated IMU data for the square trajectory in Figure 3(a). To ensure disturbances were representative of real-world conditions, a disturbance instance was obtained by sampling a real MPU-6050 while striking its mounting. IMU measurements from adding 12 disturbances to the simulated square trajectory data are shown in Figure 4.

For obtaining experimental data, the moving object was a modified model railway wagon, the smart wagon, shown in Figure 5(a) which wirelessly transmitted IMU data while powering LEDs for ground truth acquisition. To investigate the effect of the proposed method on a higher quality IMU, a second wagon shown in Figure 5(b) was additionally equipped with an Xsens MTi-610R. This higher quality IMU provided measurements at 400 Hz, had 25 times lower bias instability than the MPU-6050 and was seven times less noisy.

Ground truth position was obtained from an overhead RGB camera with low-distortion lens. Remaining lens distortion was compensated in MATLAB using a camera model.

To ensure data was captured in the locally-level frame, both the camera platform and train track were levelled using a digital inclinometer with reported accuracy of $\pm 0.1°$. Ground truth data of the smart wagon was obtained with a resolution of 0.76 mm in position and 0.01° in heading at a sampling rate of 100 Hz.

3. Results

Filter gains were optimized using an experimental data set of two and a half minutes duration in which the smart wagon travelled at speeds between 0 and 0.7 ms^{-1} around a square-shaped track measuring 1.5 m × 1.5 m. The smart wagon first performed an anticlockwise loop accelerating from 0 to 0.3 ms^{-1} and then decelerating to 0 ms^{-1} when returning to the starting point. The same trajectory was then performed in reverse and again anticlockwise before returning to the origin. In the last

Table 2. Mean sensor errors for the MPU-6050.

Sensor	Noise density	Bias instability	Rate random walk
Gyro	2.71e-04 $rads^{-1}\sqrt{Hz}^{-1}$	1.58e-05 $rads^{-1}$	1.80e-07 $rads^{-1}\sqrt{Hz}$
Accelerometer	1.50e-03 $ms^{-2}\sqrt{Hz}^{-1}$	4.40e-04 ms^{-2}	2.20e-05 $ms^{-2}\sqrt{Hz}$

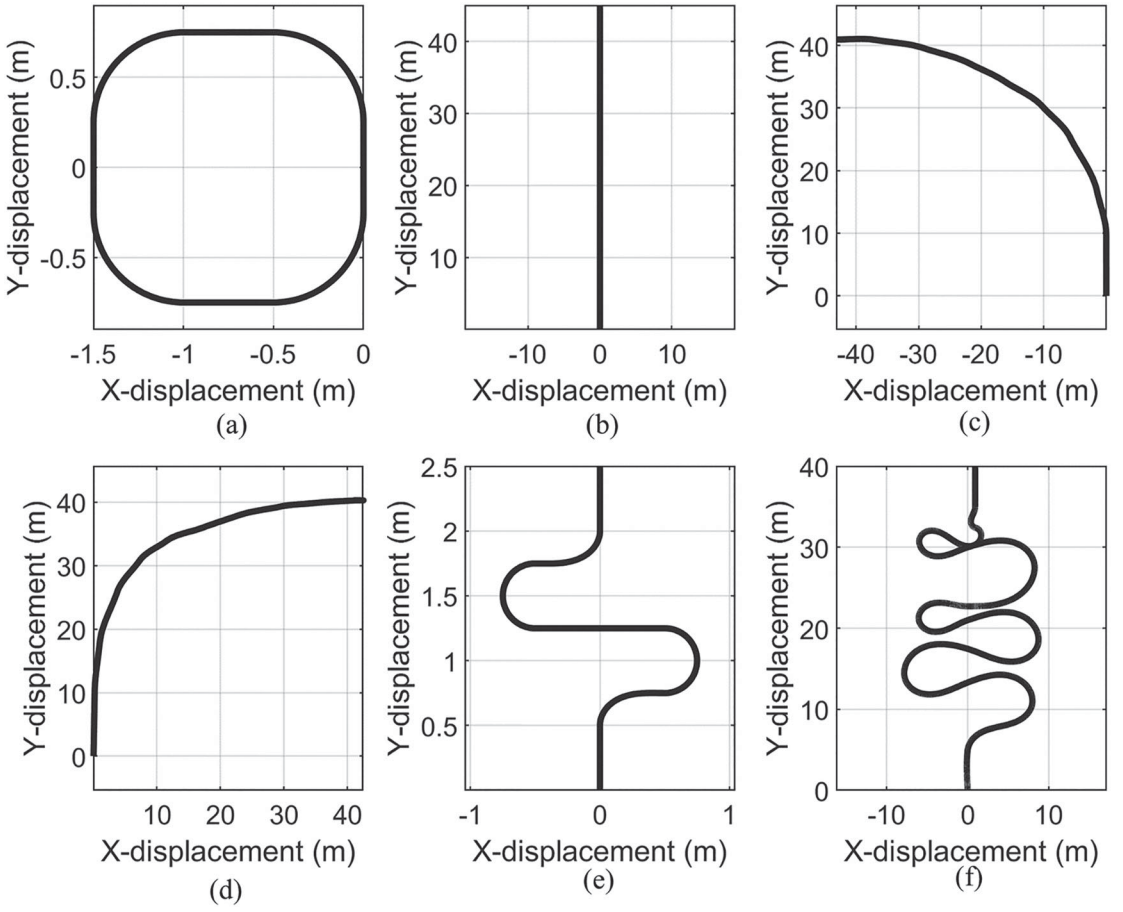

Figure 3. (a) Square, (b) straight, (c) left turn, (d) right turn, (e) s-shape, (f) zigzag trajectories.

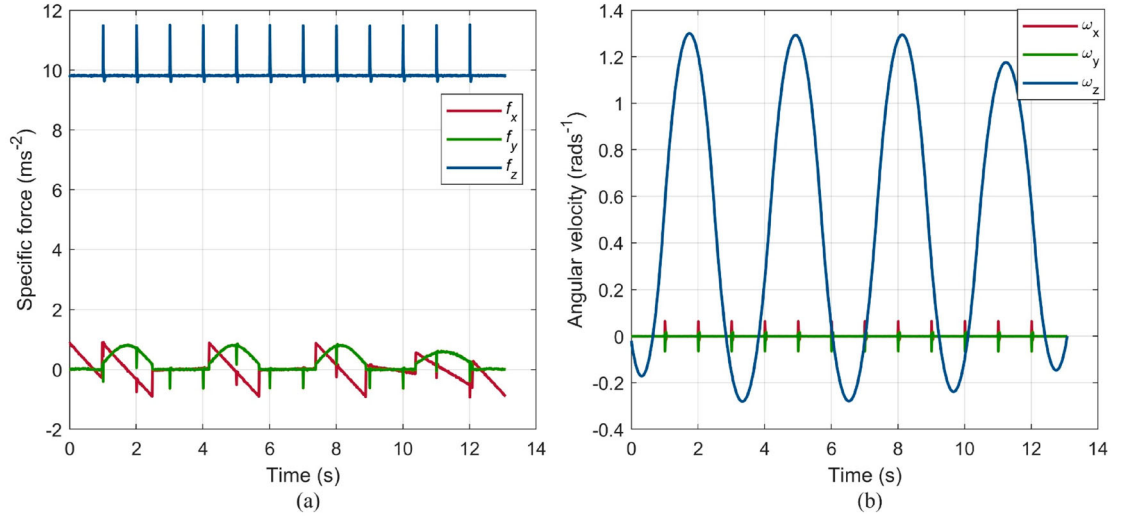

Figure 4. (a) Accelerometer and (b) gyroscope measurements with disturbances.

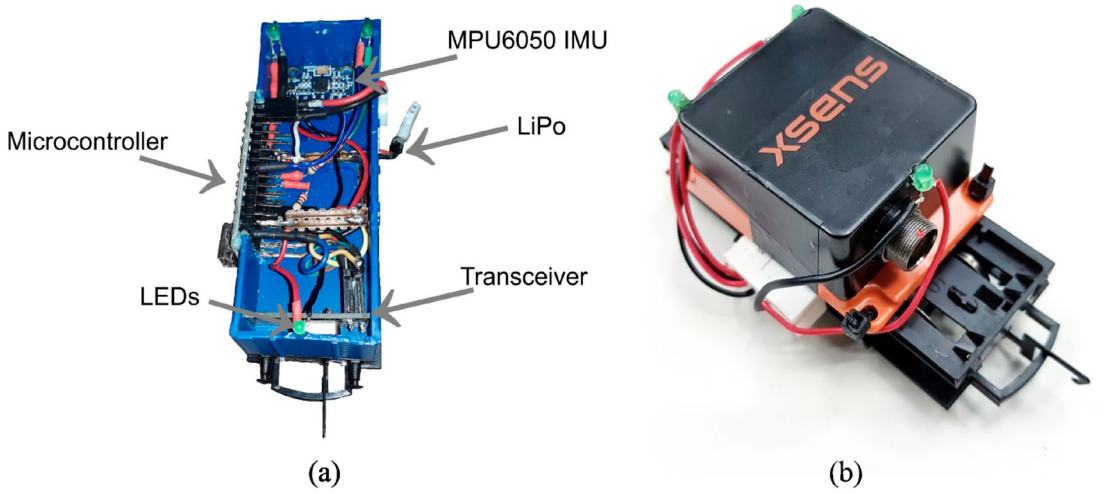

Figure 5. (a) Smart wagon and (b) Xsens wagon.

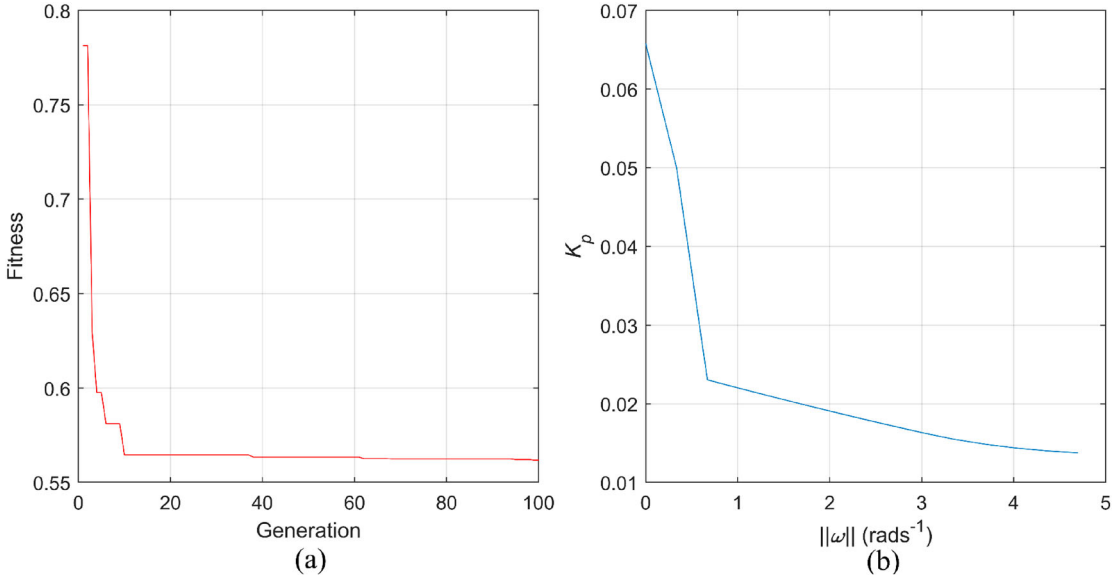

Figure 6. (a) Fitness over 100 generations and (b) input-output surface from tuned FIS.

30 s, rapid back and forth motion was performed on the straight section of track reaching a peak velocity of 0.7 ms^{-1}. This aggressive motion was induced to demonstrate the advantage of an optimally tuned gain.

Figure 6(a) shows an example of the change in fitness over 100 generations of tuning the fuzzy system. The time taken to find the optimal parameters depended on the population size, number of generations and length of data. For a population of 200, the GA completed 100 generations on a 64-core AMD EPYC™ 7543 high-performance computer in 20 min. The resulting input-output surface from the FIS is shown in Figure 6(b).

Figure 7(a) shows the cumulative distribution of mean absolute velocity errors (MAVE) for the experimental square trajectory. In Figure 7(b), the errors are shown in a box plot. To demonstrate the competitiveness of the approach, it was compared against three popular model-free orientation filters: a quaternion Extended Kalman Filter (Q-EKF), Magwick Filter and Mahony Filter. These were chosen because they were the filters used as baselines in similar works (Kottath et al., 2017; Tian et al., 2013; Wu et al., 2016). Implementations of these were obtained from the 2017 study by Michel et al. and can be found in the data availability statement. The best parameters for these filters were found by optimization using the MATLAB GA. These were the parameters which minimized the mean trajectory error on the test cases and are shown in Table 3.

The simulation data sets were used as unseen test cases to demonstrate the competitive performance of the generated model. Figures 8–13 compare the *x*-*y* velocity estimates with the ground truth of the simulated square,

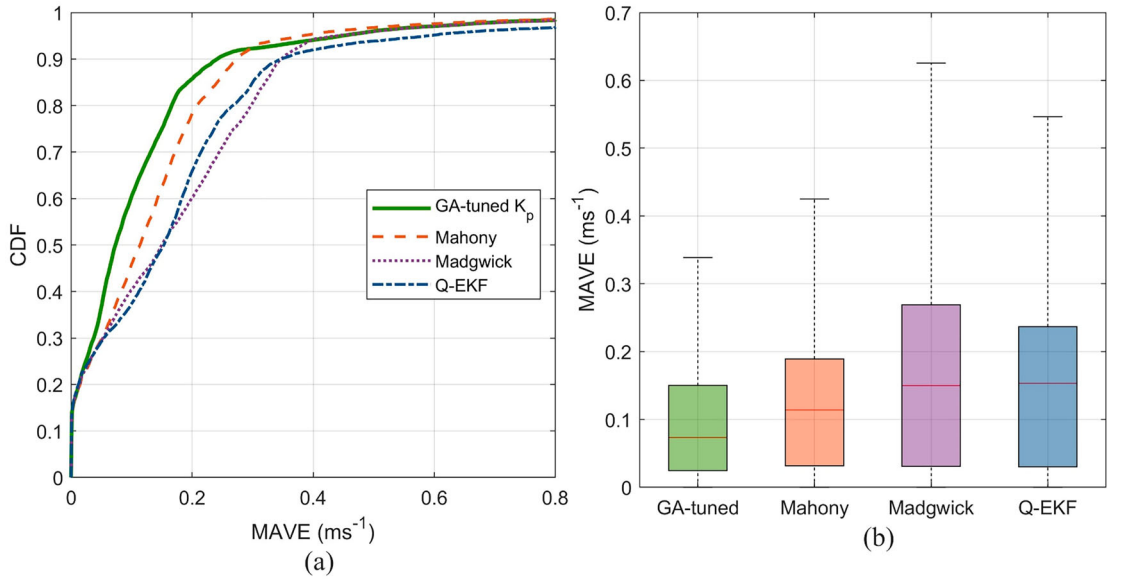

Figure 7. (a) Cumulative velocity error plot, (b) box plot for experimental square trajectory.

Table 3. Optimal parameters used for the baseline orientation filters.

Filter	Optimal parameter(s)
Madgwick	$\mu = 0.084$
Mahony	$k_p = 0.077$
Q-EKF	$\mathbf{R}_{acc} = \begin{bmatrix} 60.3^2 & 0 & 0 \\ 0 & 45.8^2 & 0 \\ 0 & 0 & 25.9^2 \end{bmatrix}$, $\mathbf{R}_{gyr} = \begin{bmatrix} 45.3^2 & 0 & 0 \\ 0 & 47.5^2 & 0 \\ 0 & 0 & 52.6^2 \end{bmatrix}$

straight, left turn, right turn, s-shaped and zigzag trajectories. Table 4 shows the WRVE and MSVE metrics for each scenario and algorithm. Figure 14 shows the trajectories obtained from integrating the velocity estimates.

To demonstrate the positive effect of adaptive k_p on trajectories containing vibrations, the trajectory of Figure 3(a) was perturbed with 12 equally spaced disturbances. The estimated trajectories for each algorithm are shown in Figure 15.

Lastly, to compare the accuracy of trajectories from a higher quality sensor, the MPU and MTi were mounted on the same wagon and performed three clockwise and anticlockwise loops of the experimental square track. Table 5 shows the MSVEs for each of these where the proposed GA-based tuning was used throughout. Figure 16 compares the trajectories obtained after integrating velocities for an anticlockwise and clockwise instance respectively.

4. Discussion

The input-output surface shown in Figure 6(b) supports the hypothesis that, for the data used in the GA's fitness function, the optimal tuning of k_p is a function that decreases monotonically with increasing $\boldsymbol{\omega}$. For quasi-stationary periods, a higher k_p puts greater weight on the correction term, $\boldsymbol{\varepsilon}$, driven by the accelerometer measurements, in updating $\hat{\mathbf{q}}_k$. During more dynamic periods, the lower k_p term intuitively places greater weight on $\boldsymbol{\omega}_{nb}^{b}$ from the gyros for updating $\hat{\mathbf{q}}_k$.

The cumulative distribution of MAVEs for the experimental trajectory in Figure 7(a) shows how the proposed method reduces velocity errors compared to the competitive filters. Although the proposed method has some errors that are marginally larger than Mahony, these are visibly outweighed by the improvements in the 30th–90th percentiles. The slight increased error for the proposed method in the 92nd–99th percentile may be due to the insufficient fidelity of the Mamdani FIS using four MFs. This could be validated by increasing the number of MFs in the input-output domains and observing the effect on the cumulative distribution of MAVEs.

Figure 7(b) shows how the median MAVE and inter quartile range are reduced by about 40% and 20% respectively with GA-tuning compared with the best performing constant gain baseline. These improvements are likely due to the increased orientation accuracy thanks to the adaptive k_p, which improves differentiation between gravity and translational acceleration due to the smart wagon's motion.

Figures 8–13 compare the *x*-*y* velocities obtained on simulated test trajectories for the GA-tuned filter and baselines. In Table 4, the GA-tuned filter is seen to reduce the mean WRVE by about 10% compared with the mean WRVEs of the three optimized constant-gain methods. The respective MSVEs show how the tuned filter achieves

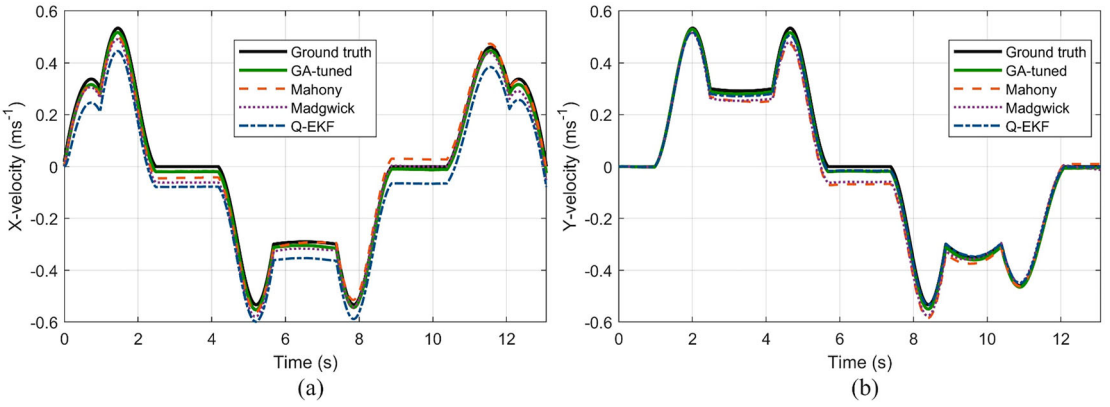

Figure 8. Plot of (a) *x* and (b) *y* velocity estimates for simulated square trajectory.

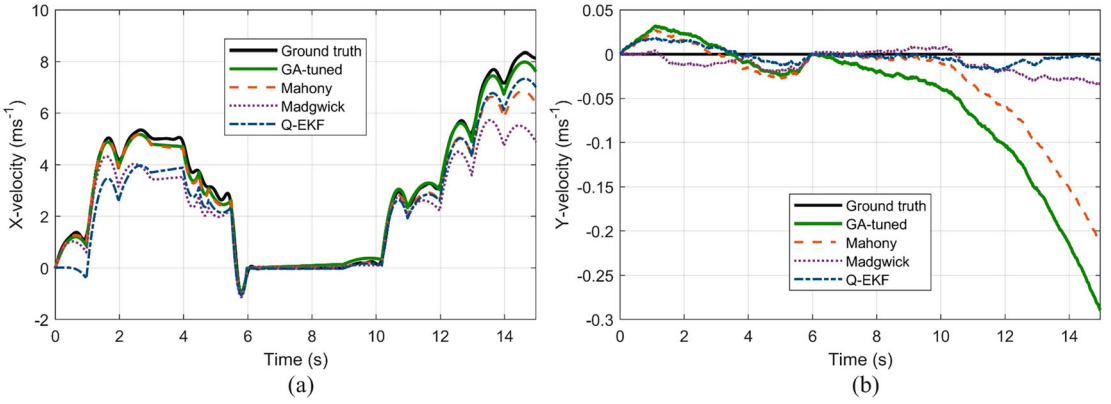

Figure 9. Plot of (a) *x* and (b) *y* velocity estimates for simulated straight line trajectory.

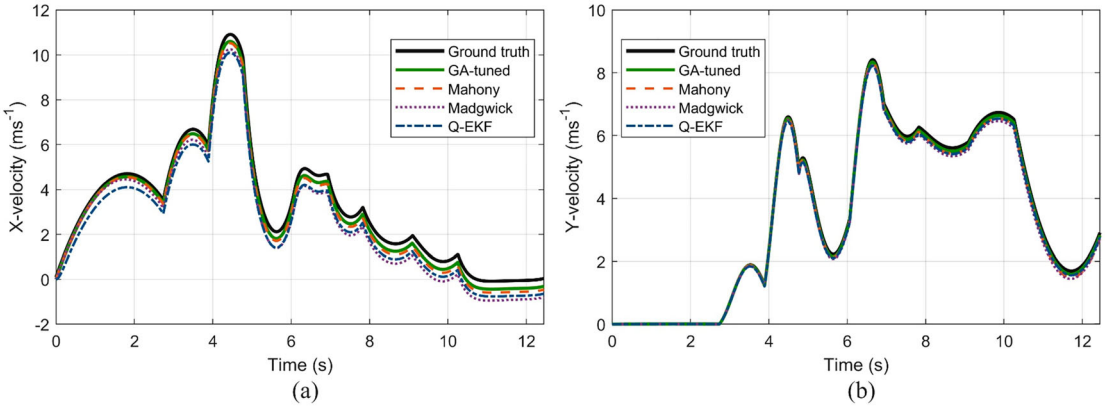

Figure 10. Plot of (a) *x* and (b) *y* velocity estimates for simulated left turn trajectory.

Table 4. Comparison of velocity errors across filters and trajectories.

	GA-tuned k_p		Q-EKF		Madgwick		Mahony	
Trajectory	WRVE (ms^{-1})	MSVE (ms^{-1})	WRVE (ms^{-1})	MSVE (ms^{-1})	WRVE (ms^{-1})	MSVE (ms^{-1})	WRVE (ms^{-1})	MSVE (ms^{-1})
Square (exp.)	0.260	0.0127	0.331	0.0165	0.412	0.0164	0.283	0.124
Square (sim.)	0.296	1.51e-04	0.309	1.84e-03	0.312	9.98e-04	0.316	9.01e-04
Square (sim.+ vibration)	0.326	2.13e-03	0.386	2.28e-03	0.357	2.22e-03	0.343	5.39e-03
Straight (sim.)	1.05	0.0141	1.39	0.223	1.20	0.415	1.10	0.0871
Left turn (sim.)	2.32	0.0298	2.77	0.234	2.45	0.176	2.36	0.0592
Right turn (sim.)	2.11	7.93e-03	2.29	0.0839	2.31	0.136	2.15	0.0225
S shaped (sim.)	0.975	4.72e-03	1.09	0.0100	1.04	9.10e-03	1.05	0.0104
Zigzag (sim.)	3.09	0.909	3.25	1.14	3.63	1.11	3.42	0.986
Average	**1.30**	**0.123**	**1.48**	**0.214**	**1.46**	**0.234**	**1.38**	**0.162**

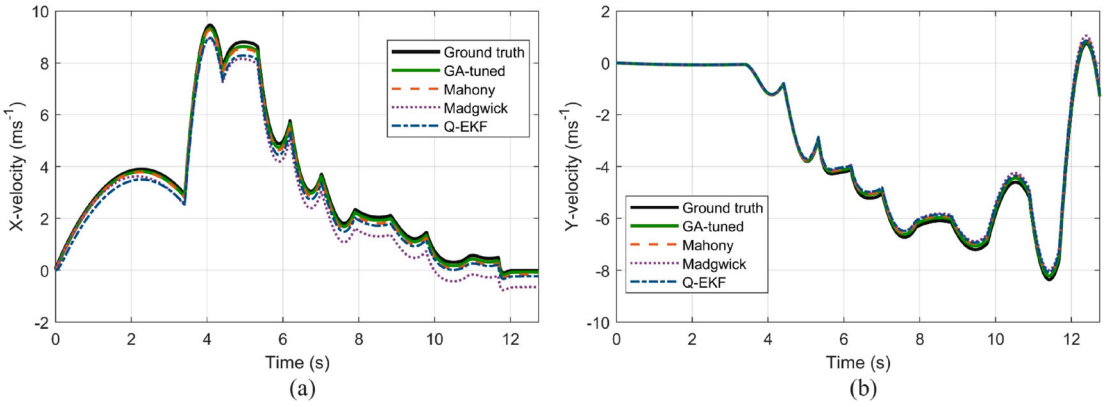

Figure 11. Plot of (a) *x* and (b) *y* velocity estimates for simulated right turn trajectory.

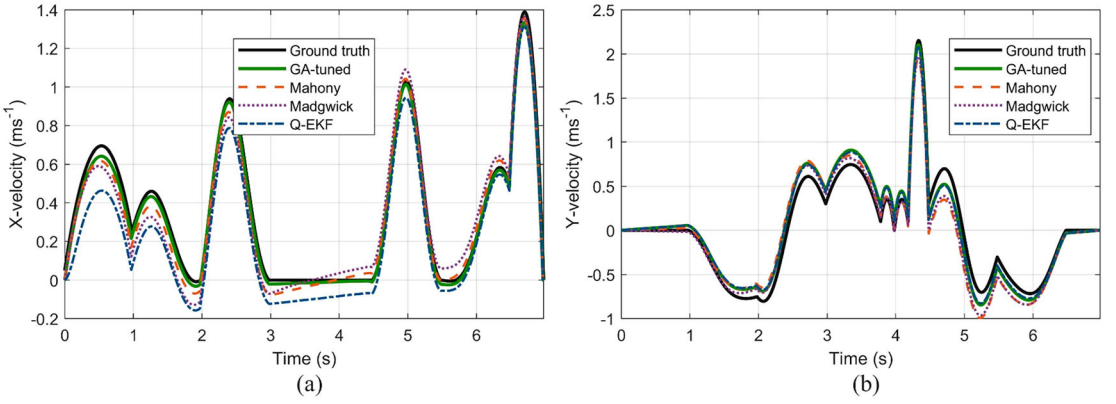

Figure 12. Plot of (a) *x* and (b) *y* velocity estimates for simulated s-shaped trajectory.

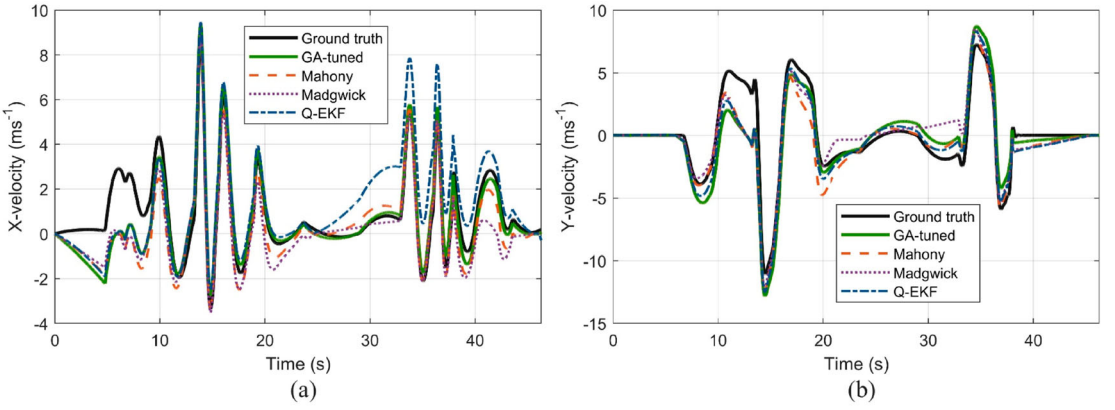

Figure 13. Plot of (a) *x* and (b) *y* velocity estimates for simulated zigzag trajectory.

Table 5. Comparison of MSVEs for the different quality IMUs.

	Clockwise			Anticlockwise			
	1 (ms^{-1})	2 (ms^{-1})	3 (ms^{-1})	1 (ms^{-1})	2 (ms^{-1})	3 (ms^{-1})	Av. (ms^{-1})
MPU	5.02e-3	0.0139	6.67e-3	1.92e-3	2.16e-3	1.82e-3	5.25e-03
MTi	2.10e-3	3.32e-04	1.29e-03	4.25e-4	2.92e-4	3.49e-4	7.98e-04

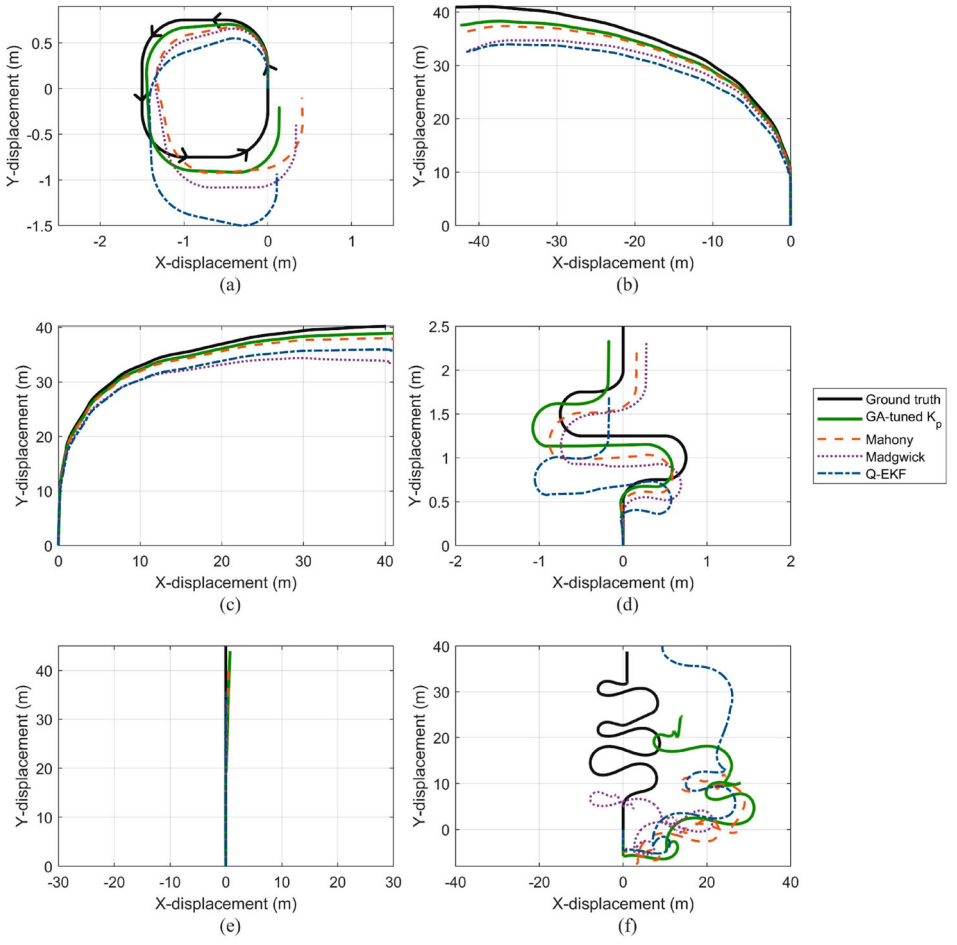

Figure 14. Estimated trajectories for the simulated (a) square, (b) left turn, (c) right turn, (d) s-shaped, (e) straight and (f) zigzag cases.

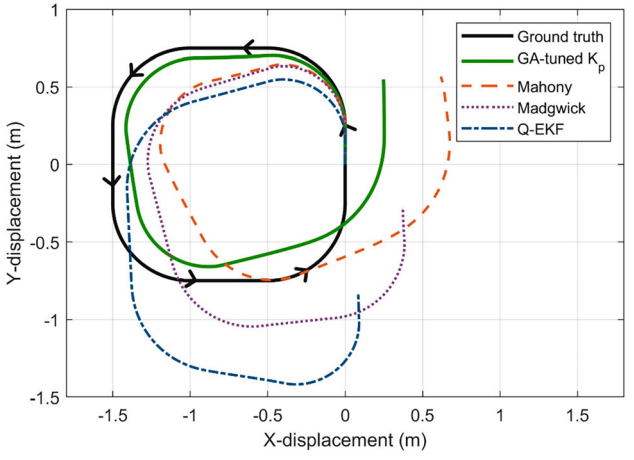

Figure 15. Estimated trajectories for the simulated square with vibration disturbances.

the lowest error for each trajectory, giving a mean MSVE about 25% lower than the best performing optimized baseline. Although only a marginal improvement in WRVE of 2% against the Mahony filter is seen in the left and right turns, this is expected as these are the least dynamic of the trajectories and hence an adaptive gain offers a small improvement. In contrast, the proposed method achieves a greater reduction in WRVE of 7% on the more dynamic zigzag trajectory. Although these improvements appear small, their positive impact after integration is shown in the trajectories in Figure 14.

Figure 15 compares the estimated trajectories obtai ned by the algorithms on the simulated square data with vibration disturbance. The proposed method is seen to be the most robust, retaining an accurate heading of the IMU for longer than the other methods. The competitive methods do not perform as well due to their constant parameters and are thus unable to reject the disturbances resulting in orientation errors.

Lastly, from Table 5 it is seen how the MTi IMU reduces the average velocity errors approximately sevenfold compared with the MPU. Comparing Figure 16(a) and (b), the MTi trajectories are seen to conform more accurately to the ground truth compared with the lower quality IMU which underestimates displacements. The most likely cause of this is error in the scale factor parameters of the MPU's accelerometers. The MTi conforms

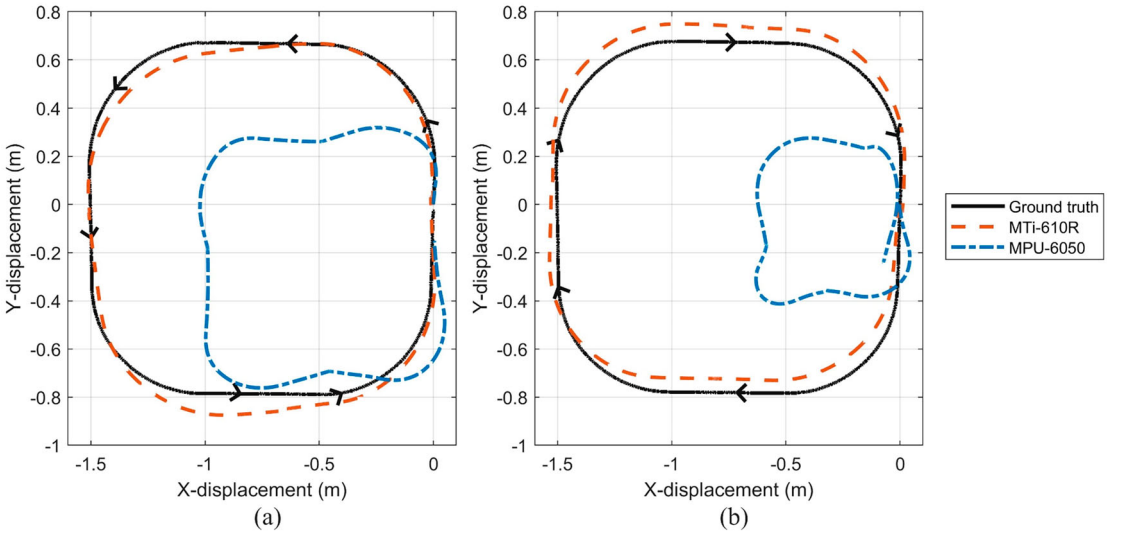

Figure 16. (a) anticlockwise and (b) clockwise trajectory for MTi and MPU IMUs.

closely to the ground truth because of the careful factory calibration of the accelerometers described in the datasheet.

Despite improvements in error metrics, large errors remain in some of the estimated velocities and resulting trajectories, particularly those in Figure 14(d,f). These trajectories being the more dynamic of the test set suggest that the limited sampling rate of 100 Hz is the primary cause of error. While 100 Hz matches the sampling rate used in the experimental data, it can cause accelerations and angular velocities of frequencies greater than the Nyquist limit to be aliased down to lower frequencies and carried along as errors in velocity and position. This is thought to be a significant contributor as, referring to Figures 12 and 13, velocity errors are induced at trajectory waypoints where sharp changes in velocity occur. This hypothesis could be validated by increasing the sampling frequency of the simulated data and analyzing the effect on the velocity error.

5. Conclusion

This work proposes the novel tuning of a complementary orientation filter by optimizing its gain using a GA. The bespoke GA is shown to compute generations faster than two competitive algorithms. After performing the parameter search on an experimental data set, the input-output surface from the resulting FIS is shown to be transparent and interpretable. The fitness of a genome is not based on orientation directly but on the error between estimated and ground truth velocities in the locally-level reference frame. The novel approach is thus termed indirect and benefits from requiring a single calibrated camera and IMU for data acquisition.

A new temporally agnostic velocity error metric, the WRVE, is also introduced. As a relative error metric, it is better suited to the inertial tracking problem because it is inherently a relative estimation (dead reckoning) method. The metric is also weighted based on the rate of turn and vibrational content of the sequence which other metrics such as the MSVE do not consider. The WRVE is thus more useful in cases where accurate velocities under highly dynamic conditions or vibrations are of interest.

The results show the GA-based tuning method reduces the average WRVE by 10% compared with the mean WRVEs of the baselines. The MSVE is reduced by 25% on average compared with the best performing constant gain filter (Mahony). The improved accuracy of velocity estimation is achieved through better differentiation between the reaction force due to gravity and translational accelerations due to motion.

Despite improvements, some of the tuned trajectories still do not come close to conforming with the ground truth. Possible causes of this include scale factor errors in the sensor models and the limited sampling rate of 100 Hz used in the data. Both can be validated by modifying the model and simulation properties and will be the subject of future work.

Due to their implicit dependence on accurate orientation, the tuning method may improve the positional tracking accuracy of other tracking methods in literature, whether based on strapdown inertial navigation or data driven. It is also a flexible approach as other parameters can be introduced and tuned by the GA such as accelerometer bias and scale factors.

Disclosure statement

No potential conflict of interest was reported by the author(s).

Funding

This research is funded by the Engineering and Physical Sciences Research Council (EPSRC) iCASE Grant reference EP/S513623/1 and BAE Systems.

Data availability statement

The data and MATLAB code that support the findings of this study are openly available to download from 10.17862/cranfield.rd.24807579. MATLAB implementations of the other orientation filters can be found at https://github.com/tyrex-team/benchmarks-attitude-smartphones/tree/master.

References

Barrau, A., & Bonnabel, S. (2017). The invariant extended Kalman filter as a stable observer. *IEEE Transactions on Automatic Control*, *62*(4), 1797–1812. https://doi.org/10.1109/TAC.2016.2594085

Bonnabel, S. (2007). Left-invariant extended Kalman filter and attitude estimation. In 2007 *46th IEEE Conference on Decision and Control* (pp. 1027–1032). IEEE.

Cai, J., Luo, L., & Hu, S. (2020). Bi-direction direct RGB-D visual odometry. *Applied Artificial Intelligence*, *34*(14), 1137–1158. https://doi.org/10.1080/08839514.2020.1824093

De Jong, K. A. (1975). *An analysis of the behavior of a class of genetic adaptive systems*. (Tech. Rep. No. 185). The University of Michigan.

El-Kebir, H., & Ornik, M. (2020). In-flight air density estimation and prediction for hypersonic flight vehicles. In *23rd AIAA International Space Planes and Hypersonic Systems and Technologies Conference*. AIAA.

El-Sheimy, N., & Youssef, A. (2020). Inertial sensors technologies for navigation applications: State of the art and future trends. *Satellite Navigation*, *1*(1), 2. https://doi.org/10.1186/s43020-019-0001-5

Fire Brigades Union. (2007). *Fatal accident investigation - Full report Into the deaths of firefighters John Averis, Ian Reid, Ashley Stephens and Darren Yates-Badley*. Fire Brigades Union. https://www.ife.org.uk/write/MediaUploads/Incident directory/Atherstone - 2007/Atherstone_FBU_Report_Full_Redacted.PDF

Gang-Qiang, G., Bo, C., Rui-Chu, C., & Yun-Shuang, W. (2023). Real-time temperature drift compensation method of a MEMS accelerometer based on deep GRU and optimized monarch butterfly algorithm. *IEEE Access*, *11*, 10355–10365. https://doi.org/10.1109/ACCESS.2023.3240766

Goodfellow, I., Bengio, Y., & Courville, A. (2016). *Numerical computation*. In *Deep learning* (pp. 78–95). MIT Press.

Groves, P. D. (2015). Navigation using inertial sensors [tutorial]. *IEEE Aerospace and Electronic Systems Magazine*, *30*(2), 42–69. https://doi.org/10.1109/MAES.2014.130191

Keki Burjorjee. (2010). *SpeedyGA: A fast simple genetic algorithm* (Version 1.22.0.0) [Computer software]. https://uk.mathworks.com/matlabcentral/fileexchange/15164-speedyga-a-fast-simple-genetic-algorithm

Kottath, R., Narkhede, P., Kumar, V., Karar, V., & Poddar, S. (2017). Multiple model adaptive complementary filter for attitude estimation. *Aerospace Science and Technology*, *69*, 574–581. https://doi.org/10.1016/j.ast.2017.07.011

Lee, Y. S., Kang, Y.-J., Lee, S.-G., Lee, H., & Ryu, Y. (2016). An overview of unmanned aerial vehicle: Cyber security perspective. *IT Convergence Technology*, *4*, 30. https://doi.org/10.21742/asehl.2016.4.30

Ludwig, S. A. (2018). Optimization of control parameter for filter algorithms for attitude and heading reference Systems. In 2018 *IEEE Congress on Evolutionary Computation, CEC 2018 - Proceedings* (pp. 1–8). IEEE.

Ludwig, S. A., & Jiménez, A. R. (2018). Optimization of gyroscope and accelerometer/magnetometer portion of basic attitude and heading reference system. In *5th IEEE International Symposium on Inertial Sensors and Systems, INERTIAL 2018 - Proceedings* (pp. 1–4). IEEE.

Madgwick, S. O. H., Harrison, A. J. L., & Vaidyanathan, R. (2011). Estimation of IMU and MARG orientation using a gradient descent algorithm. In 2011 *IEEE International Conference on Rehabilitation Robotics* (pp. 1–7). IEEE.

Madgwick, S. O. H., Wilson, S., Turk, R., Burridge, J., Kapatos, C., & Vaidyanathan, R. (2020). An extended complementary filter for full-body MARG orientation estimation. *IEEE/ASME Transactions on Mechatronics*, *25*(4), 2054–2064. https://doi.org/10.1109/TMECH.2020.2992296

Mahony, R., Hamel, T., & Pflimlin, J. M. (2005). Complementary filter design on the special orthogonal group SO(3). In *Proceedings of the 44th IEEE Conference on Decision and Control, and the European Control Conference, CDC-ECC '05* (pp. 1477–1484). IEEE.

Mahony, R., Hamel, T., & Pflimlin, J. M. (2008). Nonlinear complementary filters on the special orthogonal group. *IEEE Transactions on Automatic Control*, *53*(5), 1203–1218. https://doi.org/10.1109/TAC.2008.923738

Martínez-Soto, R., Castillo, O., Aguilar, L. T., & Rodriguez, A. (2015). A hybrid optimization method with PSO and GA to automatically design Type-1 and Type-2 fuzzy logic controllers. *International Journal of Machine Learning and Cybernetics*, *6*(2), 175–196. https://doi.org/10.1007/s13042-013-0170-8

MathWorks, Inc. (2024). *Genetic Algorithm* (Version R2023b) [Computer software]. MATLAB.

Michel, T., Geneves, P., Fourati, H., & Layaida, N. (2017). On attitude estimation with smartphones. In 2017 *IEEE International Conference on Pervasive Computing and Communications, PerCom* 2017 (pp. 267–275). IEEE.

Nazarahari, M., & Rouhani, H. (2021). 40 years of sensor fusion for orientation tracking via magnetic and inertial measurement units: Methods, lessons learned, and future challenges. *Information Fusion*, *68*, 67–84. https://doi.org/10.1016/j.inffus.2020.10.018

Noureldin, A., Karamat, T. B., & Georgy, J. (2013). *Fundamentals of inertial navigation, satellite-based positioning and their integration*. Springer Berlin Heidelberg.

Poddar, S., Narkhede, P., Kumar, V., & Kumar, A. (2017). PSO aided adaptive complementary filter for attitude estimation. *Journal of Intelligent and Robotic Systems: Theory and Applications*, *87*(3–4), 531–543. https://doi.org/10.1007/s10846-017-0507-8

Renaudin, V., Afzal, M. H., & Lachapelle, G. (2012). Magnetic perturbations detection and heading estimation using magnetometers. *Journal of Location Based Services*, *6*(3), 161–185. https://doi.org/10.1080/17489725.2012.698109

Ritchie, H., & Roser, M. (2018). *Urbanization*. Our World in Data. https://ourworldindata.org/urbanization

Shen, X., Yao, M., Jia, W., & Yuan, D. (2012). Adaptive complementary filter using fuzzy logic and simultaneous perturbation stochastic approximation algorithm. *Measurement: Journal of the International Measurement Confederation*, *45*(5), 1257–1265. https://doi.org/10.1016/j.measurement.2012.01.011

Skoglund, M. A., Hendeby, G., & Axehill, D. (2015). Extended Kalman filter modifications based on an optimization view point. In 2015 *18th International Conference on Information Fusion, Fusion* 2015 (pp. 1856–1861). IEEE.

Tian, Y., Wei, H., & Tan, J. (2013). An adaptive-gain complementary filter for real-time human motion tracking with MARG sensors in free-living environments. *IEEE Transactions on Neural Systems and Rehabilitation Engineering*, *21*(2), 254–264. https://doi.org/10.1109/TNSRE.2012.2205706

Vatter, M. (2022, June 15). Worcester cold storage and warehouse fire: Lessons and a legend emerge from tragedy: Summarizing the lessons learned from two investigations. *FireRescue1*. https://www.firerescue1.com/fatal-fires/articles/worcester-cold-storage-and-warehouse-fire-lessons-and-a-legend-emerge-from-tragedy-BhVSjRp2vmcW8rXa/

Wahlstrom, J., & Skog, I. (2021). Fifteen years of progress at zero velocity: A review. *IEEE Sensors Journal*, *21*(2), 1139–1151. https://doi.org/10.1109/JSEN.2020.3018880

Wong, C., Yang, E., Yan, X.-T., & Gu, D. (2018). Autonomous robots for harsh environments: A holistic overview of current solutions and ongoing challenges. *Systems Science & Control Engineering*, *6*(1), 213–219. https://doi.org/10.1080/21642583.2018.1477634

Wu, J., Zhou, Z., Chen, J., Fourati, H., & Li, R. (2016). Fast complementary filter for attitude estimation using low-cost MARG sensors. *IEEE Sensors Journal*, *16*(18), 6997–7007. https://doi.org/10.1109/JSEN.2016.2589660

Yun, X., Bachmann, E. R., Moore, H., & Calusdian, J. (2007). Self-contained position tracking of human movement using small inertial/magnetic sensor modules. In: *Proceedings 2007 IEEE International Conference on Robotics and Automation* (pp. 2526–2533). IEEE.

Zhang, K., Wang, C., Yu, X., Zheng, A., Gao, M., Pan, Z., Chen, G., & Shen, Z. (2022). Research on mine vehicle tracking and detection technology based on YOLOv5. *Systems Science and Control Engineering*, *10*(1), 347–366. https://doi.org/10.1080/21642583.2022.2057370

Zhang, Z., & Scaramuzza, D. (2018). A tutorial on quantitative trajectory evaluation for visual(-Inertial) odometry. In *IEEE International Conference on Intelligent Robots and Systems* (pp. 7244–7251). IEEE.